PCCP

ROYAL SOCIETY OF CHEMISTRY

REVIEW

View Article Online
View Journal | View Issue

Cite this: *Phys. Chem. Chem. Phys.*, 2025, **27**, 16717

Linking molecules to metal surfaces with covalent bonds

Weiyi Guo, Yihao Zhang and Haixing Li *

Received 26th May 2025,
Accepted 8th July 2025

DOI: 10.1039/d5cp01977j

rsc.li/pccp

Covalent linkage between organic species and metal electrodes is appealing for constructing robust and highly-conducting molecular junctions. Strategies for creating covalent organic/metal contacts often involve chemical reactions, which not only offer tools for circuitry design, but also provide rich information about surface chemistry and reaction mechanism at a molecular and atomic level. This review showcases methods including transmetalation reactions employing chemical structures such as organostannanes and boronic acids, and electrochemical redox approaches using diazonium terminal groups, as well as amines and imine radicals, for forming C–Au and N–Au bonds with Au electrodes. Other novel strategies such as $C(sp^2)$–$C(sp^2)$ bond cleavage in cycloparaphenylenes for C–Au bonds, and the well-established thiol and acetylene chemical groups for forming S–Au, S–Ag, C–Au and C–Ag bonds, are also discussed.

1. Introduction

Understanding and harnessing the electronic properties of individual molecules for potential applications in nanoscale devices is central to the field of molecular electronics.[1–5] The precise characterization and manipulation of the properties of molecular junctions have been achieved by techniques such as scanning tunnelling microscope-based break junction (STM-BJ)[6,7] and mechanically controlled break junction (MCBJ),[8,9] which enables us to create stable single-molecule circuits and obtain reproducible conductance properties of molecular junctions. Over the years, researchers in this field have been engaged in designing different chemical structures, anchoring groups, and metal electrodes for forming stable molecular circuits and investigating how the chemistry of the molecules relates to their electronic properties. Organic,[10] organometallic,[11,12] inorganic cluster,[13] peptide,[14–16] and DNA[17,18] molecules have been investigated for their single-molecule electronic properties. For metal materials, besides the commonly used Au, other metal electrodes such as Ag,[19–26] Pt,[21,24,25,27,28] Cu,[25,26,29,30] Ni,[25,31,32] Pd,[28,33] Co[25] and Zn[25] have also been applied for creating metal–molecule–metal junctions.

A significant challenge in fabricating single-molecule devices is the formation of reliable electrical contacts between target molecules and metal electrode surfaces.[34–36] The molecule/electrode contact not only provides a physical linkage between the organic structure and the metal surface but also plays an important role in mediating the electron transport; therefore, it is critical to understand the chemistry and electronic properties of different organic/metal interfaces. Among the various types of molecule–metal interactions, including dative bonds, van der Waals interactions,[37–39] ferrocene–metal interactions,[40–43] and the strong carbene–metal bond,[44–46] covalent bonds have attracted significant attention due to their ability to create stable molecular junctions with minimal contact resistance.[47,48] In addition, when graphene or carbon nanotubes are used as the electrodes, covalent bonding at the molecule/electrode interface has also been achieved,[49,50] and in some cases, has shown advantages for robust control of the conductance.[50,51] The strong electronic coupling enabled by a covalent linkage makes covalent bonding a highly favorable strategy for the development of practical single-molecule electronic components.

Department of Physics, City University of Hong Kong, Kowloon 999077, Hong Kong SAR, China. E-mail: haixinli@cityu.edu.hk

Haixing Li

Haixing Li obtained her BS in Physics from the University of Science and Technology of China. She then earned her PhD in Applied Physics at Columbia University in 2017 under the guidance of Prof. Latha Venkataraman. After graduation, she worked as a postdoctoral fellow and later a Charles H. Revson Senior Fellow in the laboratory of Prof. Ruben Gonzalez at Columbia University. She began her independent career at City University of Hong Kong in December 2021 where her research group have been investigating the fundamental charge transport properties of single-molecule circuits.

Table 1 Summary of covalent linkages between molecules and metal electrodes by different methods

Covalent linkage	No.	Termination group[a]	Condition	Ref.
C–Au	1	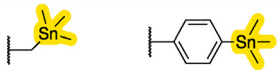	—[b]	47,48
	2	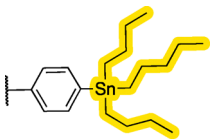	—	57
	3	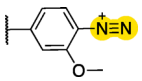	Electrochemical gating in an ionic solution with wax-coated tip for ref. 58 and 59	58–60
	4	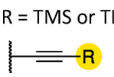	In the presence of tetrabutylammonium fluoride (TBAF)	61,62
	5	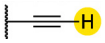	—	63–65
	6	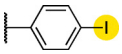	Ionic condition, wax-coated tip and negative tip bias	52
	7	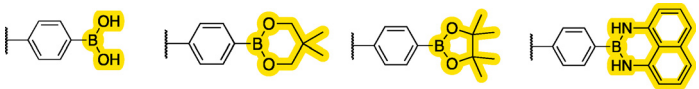	—	53,54
	8	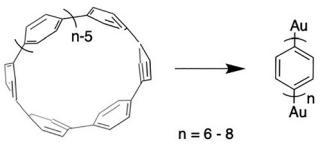	High bias voltage	66
	9	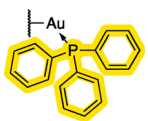	—	44,47,52
N–Au	10		In an ionic solution with wax-coated tip under high bias voltage	67
	11	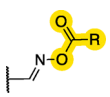	UV light exposure prior to the experiments in polar solvent with wax-coated tip	55
S–Au	12	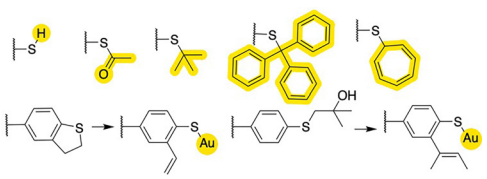	—	68–70
C–Ag	13	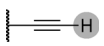	—	22,71–73
S–Ag	14		—	21

Table 1 (*continued*)

Covalent linkage	No.	Termination group[a]	Condition	Ref.
C–O–Ag	15	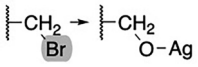	Inert atmosphere glovebox STM-BJ approach	56

[a] The highlighted parts indicate the chemical groups that are cleaved in the experiments. [b] Regular STM-BJ or MCBJ experiments with Au or Ag electrodes in a nonpolar solvent. [c] TMS stands for trimethylsilyl and TIPS stands for tri-isopropylsilyl.

Here, we overview the established covalent attachment of organic molecules onto commonly used metal electrodes, gold and silver, in forming molecular junctions. For forming a covalent bond with gold or silver, termination groups of the organic compounds undergo chemical reactions. Chemical structures of such termination groups and the corresponding reaction conditions are given in Table 1. We find that diverse chemistries of ~10 methods have been developed for forming covalent C–Au contacts, and interestingly, not all can work on both ends of an organic compound; in some systems, the molecule needs to be functionalized with one aurophilic anchoring group for an initial attachment onto one electrode for the formation of the C–Au contact on the other electrode.[52–54] Similar strategies for covalent attachment of one end of the molecule onto gold electrodes have been implemented in the formation of a N–Au covalent bond.[55] Among these covalent contacts discussed here, we find that thiol and acetylene terminal groups are the only ones that can directly form covalent bonds with either the Au or Ag electrode once they are brought into contact. The unique catalytic property of silver as shown in the measurements of α,ω-alkanedibromides will motivate more future studies in investigating the reactions at the organic/silver interface.[56] The diverse chemistry for creating covalent bonds at molecule/metal interfaces illustrates the broad applicability of gold and silver as electrode materials in molecular electronics. In the future, with a deeper understanding of the covalent organic/metal linkage and establishment of new robust contacts, more designs of molecular-scale devices will become available.

2. C–Au covalent bonding

2.1 Single-molecule junctions connected through C–Au covalent bonds on both sides

2.1.1 Cleavage of trimethyl tin terminal groups. A covalent C–Au bond for anchoring molecules onto Au electrical contacts was first achieved in 2011 (Fig. 1a).[47,48] The formation of C–Au covalently linked junctions was confirmed by the observation of the same conductance for $SnMe_3$-terminated alkanes in comparison to those of Au–PPh_3-terminated ones (Fig. 1b). The chemical structure of Au–PPh_3, which already carries the C–Au bonds at the ends, is provided in Table 1 (No. 9). Various trimethyl tin (–$SnMe_3$)-terminated molecules were shown to undergo transmetallation reaction with Au atoms to yield direct C–Au contact in forming single-molecule junctions.[47,48] For the $SnMe_3$-terminated alkane series (Fig. 1a top), an about two orders of magnitude increase in conductance was observed when compared to the amine-terminated alkanes (Fig. 1c), indicating a high electronic coupling between sp^3 hybridized carbons and Au atoms at the molecule/electrode interface. In stark contrast, for the $SnMe_3$-terminated benzene (Fig. 1a middle), conductance was only marginally increased compared with that of benzene-1,4-diamine ($0.03G_0$ *vs.* $0.008G_0$), showing that the coupling between sp^2 hybridized carbons and Au atoms was relatively weak. Notably, for the series of trimethylstannylmethyl-terminated polyphenyls (Fig. 1a bottom), an about 100× conductance increase, which is similar to that of the alkane series, was observed in comparison to the amine-terminated polyphenyls (Fig. 1d). In detail, by adding a methylene group in between the –$SnMe_3$ end group and the polyphenyl π system, the authors introduced a strongly-coupled C(sp^3)–Au contact onto a π conjugated backbone, thereby obtaining highly conducting molecular junctions. For example, the single-molecule junction conductance of 1,4-trimethylstannyl-terminated benzene nearly approached the conductance quantum ($1G_0$). Taken together, these results highlight that in the C–Au linkages, electrons mainly conduct *via* the σ channel of the carbon atoms.

2.1.2 Electrochemical reduction of diazonium terminal groups. C–Au covalent contacts have also been created at the molecule/Au interface by the electroreduction reaction of diazonium salts.[58,59,74] By applying an electrochemical gate voltage, Tao and co-workers have demonstrated that the **BP** molecule undergoes a reduction reaction at the diazonium end group, forming C–Au bonded molecular junctions (chemical structure in Fig. 1e). Specifically, junctions were formed when the applied electrochemical potential was lower than the reduction potential of the diazonium groups ~−300 mV (Fig. 1f). These covalently linked junctions showed a significantly larger junction elongation length (0.34 nm *vs.* 0.18 nm) compared with the amine-terminated analogs, which was attributed to the robustness of the C–Au covalent bonds. Later, Darwish and co-workers achieved spontaneous attachment of the same diazonium salt (**BP**) to a gold tip and silicon substrate, in which case a negative tip bias voltage is not required.[60] The authors showed that by utilizing the versatile chemistry of the diazonium salt, they created mechanically stable metal–single-molecule–semiconductor junctions.

2.1.3 Breaking C(sp^2)–C(sp^2) bonds in cycloparaphenylenes. A series of [*n*]cycloparaphenylenes ([*n*]**CPPs** (*n* = 6–8)) have been shown to undergo electrophilic aromatic substitution reaction in forming covalent C–Au contact with Au electrodes in STM-BJ experiments.[66] Under a high tip bias voltage, the

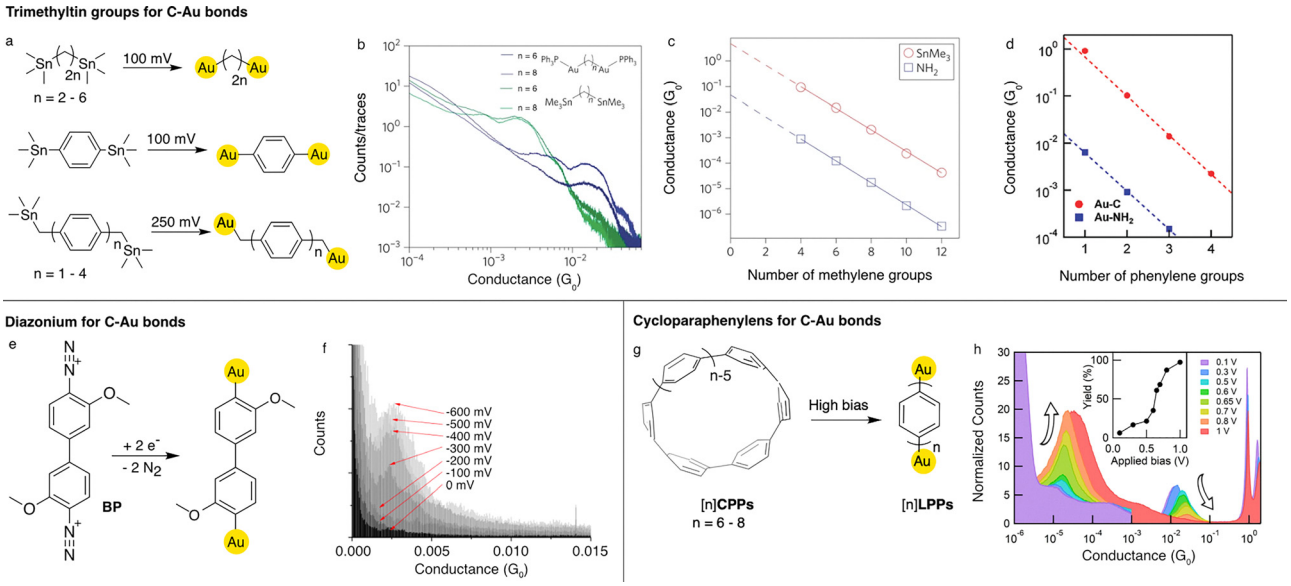

Fig. 1 (a) *In situ* C–Au bond formation by trimethyl tin cleavage reaction in single-molecule junctions under an applied electric field. (b) One dimensional (1D) conductance histograms for two $SnMe_3$-terminated and two Au–PPh_3-terminated alkanes (n = 6 and n = 8). Inset: Chemical structures for $SnMe_3$- and Au–PPh_3-terminated alkanes. (c) Conductance value on a logarithmic scale *versus* number of methylene groups in the backbone for $SnMe_3$- and NH_2-terminated alkanes. (d) Conductance *versus* number of phenylene groups in the backbone for $SnMe_3$-terminated dimethylene-*p*-polyphenyls and NH_2-terminated-*p*-polyphenyls. (e) Schematic illustration of the diazonium reduction reaction. (f) 1D conductance histograms of **BP** in a linear scale taken at electrochemical potentials *vs.* Ag/AgCl ranging from 0 to −600 mV. (g) Schematic illustration of the electric field-catalyzed electrophilic aromatic substitution reaction on [*n*]**CPP** molecules. (h) 1D conductance histograms of [6]**CPPs** measured at applied biases in the range of 0.1–1 V. Inset: The formation percentage of the low-G junctions against the applied bias. (b) and (c) are adapted with permission from ref. 47, copyright (2011) Springer Nature. (d) is reprinted with permission from ref. 48, copyright (2011) American Chemical Society. (f) is reprinted with permission from ref. 59, copyright (2013) American Chemical Society. (h) is reprinted with permission from ref. 66, copyright (2023) Springer Nature.

hoop-shaped conjugated π-complex ([*n*]**CPP**) underwent an electrophilic aromatic substitution reaction to form a charge-separated linear oligophenylene ([*n*]**LPP**) that was spontaneously linked to the Au tip and substrate through covalent C–Au bonds (Fig. 1g). As shown in Fig. 1h, under tip bias voltages of lower than 0.5 V, the conductance peak at $\sim 2 \times 10^{-2} G_0$ (high-G) indicates that a direct Au–π coupled junction between the Au atoms and the conjugated π-complex was formed in the measurement of [6]**CPP**. When the applied tip bias exceeded 0.5 V, a lower conductance peak (low-G) at $\sim 5 \times 10^{-5} G_0$ appeared (Fig. 1h), suggesting that the high bias-catalyzed C–C cleavage leads to the formation of two covalent C–Au bonds at both ends, thus the formation of [6]**LPP** junctions. It is noteworthy that a highly efficient [*n*]**CPPs** to [*n*]**LPPs** conversion was achieved under ambient conditions with a bias voltage of ∼0.7 V in a nonpolar solvent environment.

2.1.4 Protected terminal acetylenes. An alternative strategy to create covalent C–Au contacts involves the use of alkynes.[61–65] By exploring a series of trimethylsilyl (TMS)-terminated oligo-(phenylene ethynylene)s (**OPEs**), Wandlowski and co-workers demonstrated that the TMS group attached to an alkynyl group was cleaved *in situ* in the presence of tetrabutylammonium fluoride (TBAF), thereby creating covalent C–Au bonds (Fig. 2a).[61] Distinct conductance peaks were observed at $1.6 \times 10^{-2} G_0$, $2.0 \times 10^{-3} G_0$, and $2.5 \times 10^{-4} G_0$ for the measurements of **OPE1**, **OPE2**, and **OPE3**, respectively (Fig. 2b), which were attributed to be signatures for the C–Au covalently linked single-molecule junctions. These findings, showcasing examples of three different molecular backbone designs, demonstrate the use of a TMS group with added TBAF as a robust method for creating a C–Au contact at the molecule/metal interface.

Furthermore, Huang *et al.* designed a cruciform molecule **M1** consisting of two orthogonally arranged π-conjugated systems.[62] Within the structure of the molecule, one linear arm was terminated with pyridyl groups, which can bind to the Au surface through a dative N→Au bond to form **M1**-N molecular junctions. The other arm was capped with triisopropylsilyl (TIPS)-protected acetylene groups. Only when TBAF was added to the solution in an MCBJ experiment, the TIPS groups were cleaved, leading to the formation of the C–Au covalently linked **M1**-C junctions (illustration of **M1**-N and **M1**-C junctions are shown in Fig. 2c). The authors also synthesized a control molecule **M2** and realized the desilylation reaction in MCBJ measurements to generate the covalently linked **M2**-C junction (Fig. 2d). The conductance peak of **M1**-C was at the same position as that of **M2**-C, providing evidence for the junction geometry for the **M1** measurement in the presence of TBAF (Fig. 2e). Taken together, the one order of magnitude increase in conductance for **M1** measured in the presence of TBAF compared to that measured in the absence of TBAF indicates that two different molecular junctions with distinct charge-transport properties are achieved.

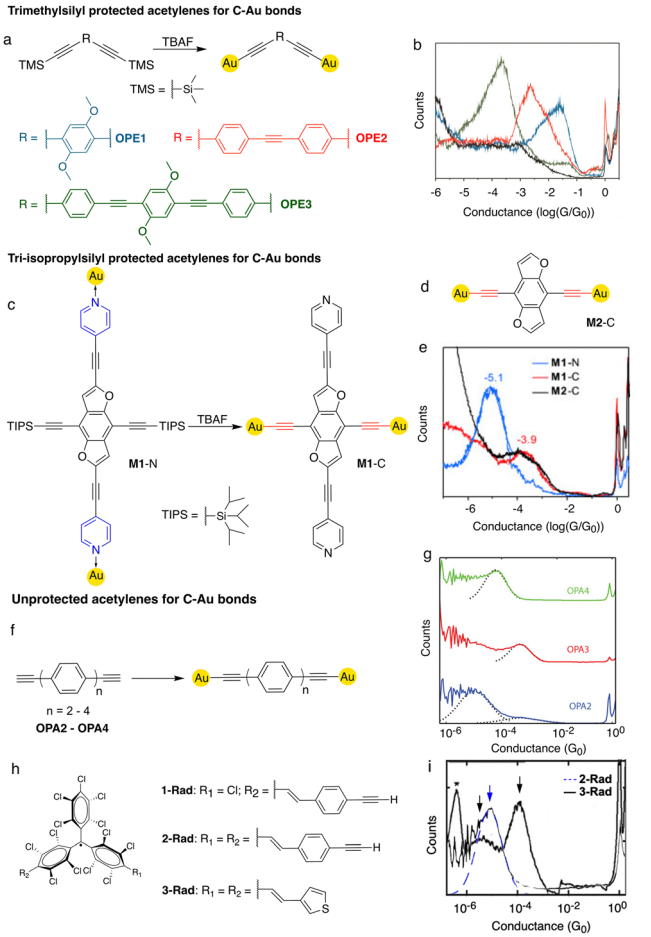

Fig. 2 (a) *In situ* C–Au bond formation by TMS-group cleavage in the presence of TBAF in single-molecule junctions. (b) 1D conductance histograms of **OPE1**, **OPE2**, and **OPE3**. (c) *In situ* single-molecule junction conversion from **M1**-N to **M1**-C by TIPS-group cleavage in the presence of TBAF. (d) Chemical structure of the **M2**-C single-molecule junction. (e) 1D conductance histograms of **M1**-N, **M1**-C, and **M2**-C. (f) Schematic illustration of *in situ* deprotonation of alkynyls in forming C–Au bonds. (g) 1D conductance histograms for **OPA2**, **OPA3**, and **OPA4**. The dashed lines represent log-normal fit around the peaks and are used to determine the conductance value. (h) Chemical structure of the PTM radicals, **1-Rad**, **2-Rad**, and **3-Rad**. (i) 1D conductance histograms for **2-Rad** and **3-Rad**. The blue dashed line represents log-normal fit to the data of **2-Rad** around the conductance region displaying molecular features. (b) is adapted with permission from ref. 61, copyright (2012) American Chemical Society. (e) is reprinted with permission from ref. 62, copyright (2015) Wiley-VCH. (g) is reprinted with permission from ref. 63, copyright (2016) American Chemical Society. (i) is reproduced with permission from ref. 64, copyright (2018) American Chemical Society.

2.1.5 Unprotected terminal acetylenes. Pla-Vilanova *et al.* demonstrated, for the first time, that unprotected terminal alkynes can spontaneously bind to the Au surface through C–Au bonds.[65] The authors showed spontaneous formation of C–Au bonds without the use of deprotonation agents or external stimuli. In their study, a gold STM tip and self-assembled monolayers (SAMs) containing 1,4-diethynylbenzenes were fixed at a specific tunneling distance, and molecular junction formation was detected by sudden jumps in the measured tunneling current. Notably, with the same benzene backbone, the lifetime of alkyne-linked junctions was slightly shorter than that of thiol-linked ones while exceeding that observed for amine-linked ones, indicating a robust C–Au contact.

Olavarria-Contreras *et al.* further realized C–Au covalent contacts without the need for an additional chemical group to protect the alkynyl carbon on a series of alkynyl-terminated oligophenylenes (**OPAs**) (chemical structure in Fig. 2f).[63] Single-molecule conductance measurements were performed using the MCBJ technique. The well-defined conductance peaks (Fig. 2g) indicate a robust molecule/metal contact formation through the use of an alkynyl end group; this was again demonstrated in later studies by other research groups.[22] For **OPA2**, two conductance peaks are detected, with the high conductance state corresponding to the molecular conductance of the molecule itself, while the low conductance feature is associated with the formation of dimers of **OPA2**.

Crivillers and co-workers further expanded the molecular design of C–Au linked metal–molecule–metal junctions by including an organic paramagnetic moiety in the center. The authors employed the perchlorotriphenylmethyl (PTM) radical as the molecular backbone, and this radical is stable under ambient conditions (chemical structure in Fig. 2h).[64] The authors applied *ex situ* characterization techniques including X-ray photoelectron spectroscopy (XPS), electron paramagnetic resonance spectroscopy (EPR), and Raman spectroscopy to study the self-assembled monolayers (SAMs) of **1-Rad** on Au, and confirmed the creation of a covalent molecule–metal linkage at the SAMs/Au interface. Importantly, the magnetic character of the functional PTM radicals was demonstrated to be maintained after the formation of the covalent linkages. The single-molecule conductance measurement of **2-Rad** showed that robust molecular junctions were formed with the Au electrodes, likely through the C–Au bond (Fig. 2i). A double-peak signature was observed in the conductance measurement of **3-Rad**, a compound equipped with thiophene terminal groups (chemical structure in Fig. 2h). The authors attributed the two peaks to be resulting from two molecule–metal contact geometries and weak S–Au linkages. On the other hand, the narrow peak of **2-Rad** indicates a well-defined interface geometry of the robust C–Au covalent bond.

2.2 Single-molecule junctions with a covalent C–Au bond on one end and a dative bond on the other

2.2.1 Oxidative addition of aryl iodides. Certain chemical groups, such as iodides and boronic acids, when used as linker groups on both ends of a molecular backbone, cannot spontaneously cleave in the presence of Au electrodes for forming molecular junctions. When the molecule is terminated with a robust gold-binding group such as thiomethyl on one side, then equipped with an iodide or boronic acid on the other side, molecular junctions are formed. Below we discuss such unique designs of terminating a molecule with two different linker groups on the two ends for establishing robust interactions between individual molecules and gold electrodes. In Fig. 3a, oligophenylenes terminated with an iodide on one end and a thiomethyl group on the other (**I1–I4**) were studied using the

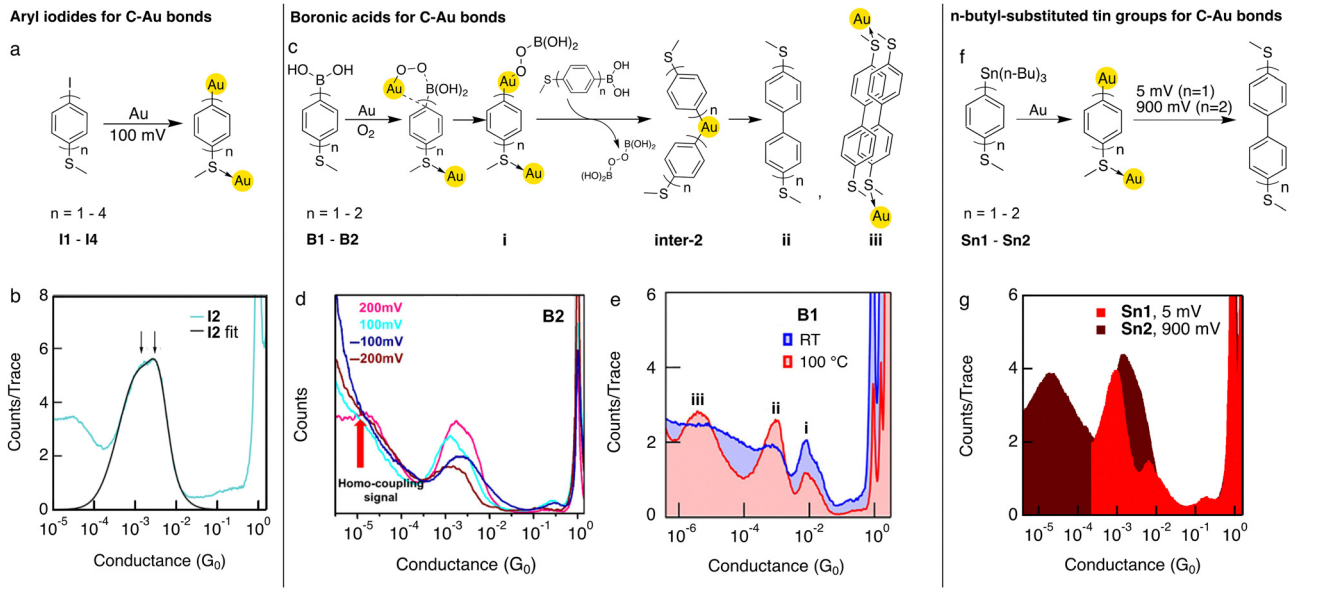

Fig. 3 (a) Schematic illustration of *in situ* cleavage of aryl iodides in forming junctions with C–Au covalent linkage on one side and a S→Au dative bond on the other. (b) 1D histogram of **I2** measured under 100 mV in TCB. The black line represents a double Gaussian fit to the data. (c) Proposed mechanism of *in situ* cleavage of the organoboron group, homocoupling reaction, and proposed molecular junction for the ultra-low conductance peak labeled as **iii**. (d) 1D conductance histograms of **B2** measured under bias voltages of 200 mV, 100 mV, −100 mV, and −200 mV. (e) 1D conductance histograms of **B1** measured in bis(2-ethylhexyl) adipate solvent under room temperature and 100 °C. (f) Schematic illustration of *in situ* cleavage of the organotin group and homocoupling reaction. (g) 1D conductance histograms of **Sn1** and **Sn2** measured in TCB under 5 mV and 900 mV bias voltages. (b) is adapted with permission from ref. 52, copyright (2020) American Chemical Society. (d) is adapted with permission from ref. 53, copyright (2022) Chinese Chemical Society. (e) is adapted with permission from ref. 54, copyright (2024) American Chemical Society. (g) is adapted with permission from ref. 57, copyright (2024) American Chemical Society.

STM-BJ technique.[52] The conductance histogram of **I2** measured in a nonpolar solvent TCB exhibits a broad conductance peak and is fitted to a double Gaussian function. The authors proposed that two different junctions contribute to the broad conductance peak: the low conductance feature arises from molecular junctions formed through a donor–acceptor I→Au bond on one side, and the high conductance feature corresponds to molecular junctions connected through an C–Au covalent contact on one side (indicated by the two arrows in Fig. 3b); in both cases the other side of the molecule is attached to the electrode through a S→Au interaction. This covalent C–Au bond was created upon the iodide cleavage on the Au surface. Further conductance measurements were performed in an ionic environment with a wax-coated tip, as under such conditions, a dense electric double layer is formed at the tip but not at the substrate; thereby, reactions are likely occurring at the tip/solution interface. Under this assumption, these experiments revealed that the formation of an I→Au dative linkage on the tip is favored when a positive tip bias is applied, and a negative tip bias promotes the formation of the covalent C–Au bond. The authors explained that the tip is electron deficient at positive bias, and both I→Au and C–Au contacts exist at the tip. Conversely, under negative bias, the tip becomes electron-rich, which is more likely to engage in oxidative addition with the aryl iodide group, leading to the formation of the C–Au bond. Therefore, this iodide cleavage reaction can be regulated by adjusting the applied bias polarity in an electrochemical environment.

2.2.2 Transmetalation of aryl boronic acids. Furthermore, Li *et al.* reported, for the first time, that by using the thiomethyl linker group on one side and a boronic acid group on the other, a transmetalation reaction of boronic acid group occurs, leading to the formation of a C–Au covalently linked product (labeled as **i** in Fig. 3c), as was monitored *in situ* by the STM-BJ technique.[53] As shown in the histograms of **B2** in Fig. 3d, the authors additionally show that only when a tip bias voltage was increased to above 200 mV, a second low conductance peak appears, which is attributed to a junction of a homocoupled dimer (labeled as **ii** in Fig. 3c). The authors suggested the following reaction mechanism as laid out in Fig. 3c. The charged Au tip first interacts with the adsorbed O_2 to form the oxidized Au. A boronic acid group was then replaced by the positively charged Au and produces the initial transmetalation intermediate **i**. Due to the increased electrophilicity of the Au tip under a high bias voltage, a second transmetalation occurs at this intermediate and leads to the formation of an Au bridged intermediate (labeled as **inter-2**). This **inter-2** undergoes a reductive elimination step, yielding the homocoupling product **ii**. This reaction was further studied in a later work by Inkpen and co-workers.[54] The authors showed that although for **B1**, homocoupling reaction does not seem to occur in room temperature STM-BJ experiments, agreeing with the Li *et al.* results, this homocoupling reaction occurs at a reasonable efficiency under 100 °C as indicated by the clear single-molecule conductance signature (Fig. 3e). Additionally, an

ultra-low conductance peak (labeled as **iii**) was observed, which was ascribed to the junctions formed by two π–π stacked homocoupling products (illustration of the **iii** junction is shown in Fig. 3c). This result highlights that the use of heat is another effective means for promoting chemical reactions in single-molecule junctions.

2.2.3 Cleavage of *n*-butyl-substituted tin groups. Based upon prior work of using the cleavage of a trimethyltin group for creating C–Au contact, Li and co-workers achieved both an effective C–Au bond formation and C–C homocoupling reaction with a group of polyphenylene molecules terminated with an *n*-butyl-substituted tin group on one end and a thiomethyl group on the other (Fig. 3f).[57] In the conductance histograms shown in Fig. 3g, **Sn1** and **Sn2** both show two peaks, arising from the efficient formation of the covalently linked monomer (high conductance) and a homocoupled dimer junction (low conductance). In the case of **Sn1**, a biaryl compound was formed from homocoupling reaction under a bias potential as low as 5 mV.

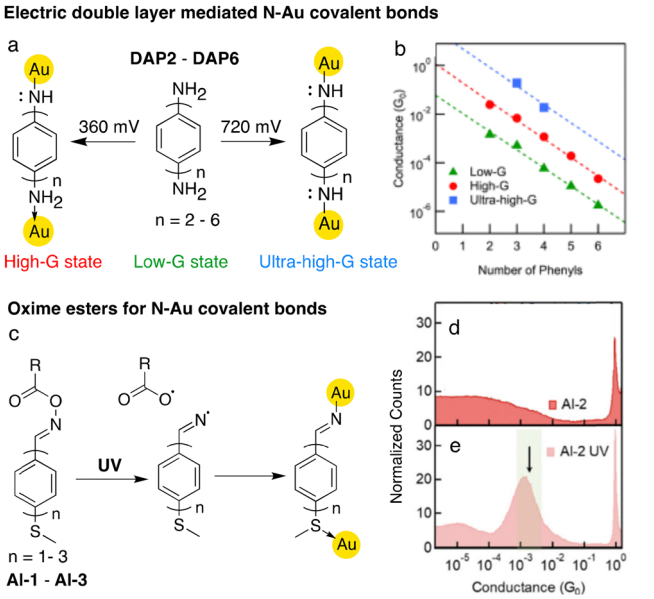

Fig. 4 (a) Schematic illustration of the formation of the novel N–Au contact upon oxidation of a dative N→Au bond under high bias voltage in an ionic environment with a wax-coated STM tip. (b) The most probable conductance values, determined from Gaussian fits to peaks in 1D conductance histograms, as a function of the number of phenylene units in the molecular backbone. Data were acquired at a constant tip bias of 90 mV for low-G, either 360 or 720 mV for high-G, and 720 mV for ultra-high-G. Dashed lines are linear fits to these data. (c) Illustration of the iminyl radical-Au covalently bonded single-molecule junctions. 1D conductance histograms of (d) **Al-2** and (e) UV-light-treated **Al-2** measured in propylene carbonate (PC) with a wax-coated STM tip under a tip bias voltage of 0.5 V. (b) is reprinted with permission from ref. 67, copyright (2017) American Chemical Society. (d) and (e) are adapted with permission from ref. 55, copyright (2023) American Chemical Society.

3. N–Au covalent bonding

3.1 Oxidation of amines

In addition to C–Au covalent linkages, several methods have been successfully established for creating another type of covalent linkage: N–Au bonds. Venkataraman and colleagues demonstrated the formation of a stable N–Au bond within an ionic environment by utilizing oligophenylene molecular wires terminated with amine groups.[67] These amine-terminated compounds were previously shown to exhibit one conductance peak,[75–77] corresponding to single-molecule junctions linked by amine-Au donor–acceptor bonds. Research by Venkataraman and co-workers here revealed that in an ionic environment, these molecular systems showed three distinct conductance states, which were assigned to single-molecule junctions with altered chemical interactions at the molecule/metal interface (Fig. 4a). A semilogarithmic plot of conductance value *versus* the number of phenylene units in the molecular backbone (Fig. 4b) showed a decay constant of $\beta \approx 1.8$ per phenyl unit for all three states, indicating that charge transport is predominantly governed by the π-conjugated oligophenylene backbone across all conductance states. Therefore, the distinction between the three conductance states lies in the metal–molecule contact configuration. The high-G state occurred under a high positive tip bias (~360 mV) in an ionic environment, whereas the ultra-high-G state appeared at even higher biases (~720 mV). The authors proposed that, under high-bias voltage, nitrogen's lone pair donates one electron to Au, resulting in the loss of a proton from the amine group. This process of removing one electron and one proton from the junction leads to the transformation of a dative N→Au bond into a more conductive N–Au bond. The emergence of the ultra-high-G state was thus explained by the transformation of both dative N→Au bonds into covalent N–Au contacts. Through the formation of robust molecular junctions in an oxidizing ionic medium with primary amine linkers, the authors demonstrated a new method for achieving low contact resistance in single-molecule devices.

3.2 Iminyl radicals

The reaction between organic radicals and transition metals can also lead to the formation of a covalent contact. For instance, using the STM-BJ technique, Zang and co-workers reported that a N–Au covalent contact was formed from the reaction between iminyl radicals and Au electrodes at the single-molecule level. The authors demonstrated that the photochemical homolysis of the N–O bond produces free iminyl radicals, which subsequently forms a N–Au bond when brought into contact with Au electrodes (Fig. 4c).[55] The 1D conductance histograms depicted in Fig. 4d and e corroborate that highly conductive single-molecule junctions were formed only when the molecules were treated with UV light irradiation prior to the measurements, indicating that the iminyl radicals generated upon UV exposure were indispensable for junction formation.

4. S–Au covalent bonding

4.1 Varied substituent groups in aryl thioethers

It has been widely reported that thiol- (–SH)[6,80,81] as well as thioacetyl- (–SAc)[82–85] terminated compounds form S–Au covalent

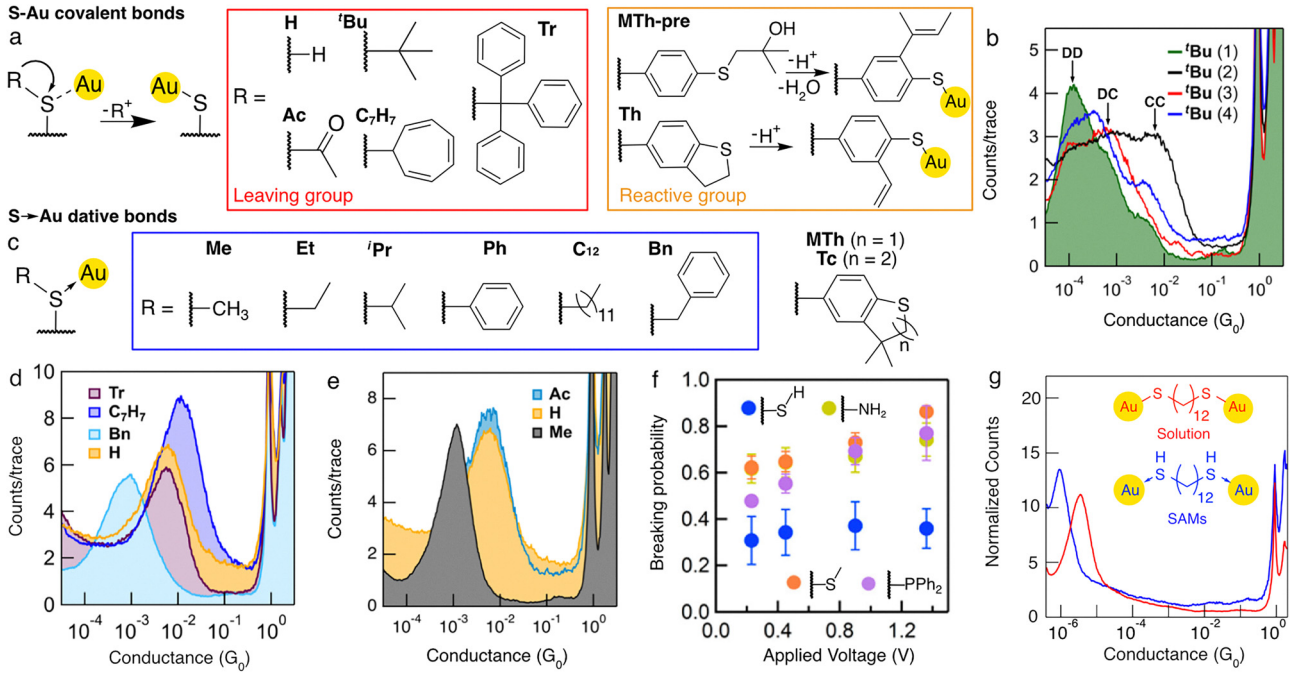

Fig. 5 (a) Illustration of the formation of the covalently bonded single-molecule junctions when different thioether termination groups are used. (b) 1D conductance histograms of **^{t}Bu** (biphenyl terminated by thio-*tert*-butyl groups) obtained from four independent STM-BJ measurements; experimental variation is visible. The arrows indicate the locations of the molecular conductance peaks. (c) Structures of the chemical groups that form S(R)→Au dative bonds with Au electrodes. (d) 1D conductance histograms of **Tr**, **C_7H_7**, **Bn** and **H** analytes (biphenyl backbone terminated with corresponding terminal groups) measured in TCB under a tip bias voltage of 100 mV. (e) 1D conductance histograms of **Ac**, **H**, and **Me** analytes (biphenyl backbone terminated with corresponding terminal groups) measured under the same condition as that in Fig. 5d. (f) The relation between junction breaking probability and the applied bias voltage for analytes equipped with covalent (blue) or dative (orange, yellow, and purple) end groups. (g) 1D conductance histograms of dodecane-1,12-dithiol obtained from STM-BJ experiments on a solution or self-assembled monolayers (SAMs) under a tip bias voltage of 345 mV. Inset: Chemical structures of the single-molecule junctions formed in the solution and SAMs. (b) and (e) are adapted with permission from ref. 68, copyright (2024) American Chemical Society. (d) is adapted with permission from ref. 69, copyright (2025) American Chemical Society. (f) is adapted with permission from ref. 78, copyright (2015) American Chemical Society. (g) is adapted with permission from ref. 79, copyright (2019) Springer Nature.

contacts with Au electrodes. The mechanism for the formation of covalent S–Au contact using –SR functionalized compounds is illustrated in Fig. 5a. A prerequisite for the creation of a covalent S–Au bond is the formation of a stable carbocation leaving group. In a recent work, Prana *et al.* studied a wide range of substitution groups (R) in the terminal thioether (–SR) group and identified a new thioether group, *tert*-butylthiol (^{t}Bu), that can form covalent bonds with gold surfaces.[68] The experimental results for 4,4′-bis(*tert*-butylthio)-biphenyl reveal three distinct conductance features, as indicated by the arrows in Fig. 5b. The authors attributed the high conductance peak to be the signature for junctions with covalent S–Au bonds on both sides (CC), the low conductance peak to junctions with two intact dative S(**^{t}Bu**)–Au linkages (DD), and the intermediate conductance feature to **^{t}Bu** junctions consisting of one dative and one covalent linkage (DC). Additionally, **MTh-pre** (structure is given in Fig. 5a) was suggested to undergo a ring closing reaction, followed by a ring opening reaction, and ultimately form a S-Au covalent contact (detailed discussions are provided in ref. 68). Importantly, the results show significant variations across independent measurements, which the authors ascribed to a phenomenon due to differences in gold surface roughness, *i.e.* different number of undercoordinated Au atoms present at the molecule/Au interface. In a follow-up study from the same team, the authors further explored two additional –SR anchoring groups where the substitution group (R) is triphenylmethyl (**Tr**) or cycloheptatrienyl (**C_7H_7**).[69] The results revealed that in both cases, molecules are attached to the Au electrodes through covalent S–Au bonds (Fig. 5d). Notably, junctions formed from **C_7H_7** showed an even higher conductance value than those formed from **H**, which needs further investigation. In a separate study, another cyclic thioether **Th** (structure is given in Fig. 5a) was shown to undergo a ring opening reaction and form a covalent S–Au bond after 24 h in the presence of tetrahydrofuran (THF) or immediately with the addition of trifluoroacetic acid (TFA).[70] Reaction schemes for the ring opening of **Th** in forming the S–Au bond with Au electrodes were discussed extensively in previous works.[68,70]

From measurements of **Ac**, **H**, and **Me**, 4,4′-biphenyl backbones terminated with thioacetyl, thiol, and thiomethyl linker groups respectively, the authors showed that both **Ac** and **H** exhibit conductance values higher than that of **Me** by a factor of 6 (Fig. 5e), suggesting that a S–Au covalent linkage is more conductive than a S(R)–Au dative linkage. Consistent with prior observations for **Me**, a low-conductance feature was identified at $\sim 10^{-3} G_0$ in the measurement of the benzyl-terminated derivative (**Bn**), suggesting the formation of dative contacts between the

molecules and gold electrodes (Fig. 5d). In addition to thiomethyl, the authors investigated other –SR groups where only dative S(R)–Au bonds are formed (chemical structures are provided in Fig. 5c); for example, when the substituent (R) is methyl (**Me**), ethyl (**Et**), isopropyl (**^{i}Pr**), phenyl (**Ph**), dodecyl (**C_{12}**), or benzyl (**Bn**) as well as cyclic thioether groups such as 3,3-dimethyl-2,3-dihydrobenzo-[*b*]thiophene (**MTh**) and 4,4-dimethylthiochromane (**Tc**). Importantly, after the authors investigated all of the above-mentioned sulfur-based anchor groups, they found that the single-molecule conductance is influenced by the choice of the substitution R group, even when the same type of S(R)–Au dative contact is formed between the molecule and the gold atoms.

Furthermore, Venkataraman and co-workers examined the stability of various molecule/gold contacts in single-molecule junctions by evaluating the breaking probability of single-molecule junctions under an applied voltage.[78] A single-molecule junction was held at a fixed electrode–electrode distance for 150 ms under an applied bias and junctions with a conductance value lower than the noise floor at the end of this 150 ms period were determined to be broken. Thousands of junctions were analyzed by this method, and among the four tested molecules, junctions formed from thiol-terminated hexane exhibited the lowest rupture probability, which remains low up to an applied voltage of 1.4 V (blue dots in Fig. 5f). In contrast, analogous junctions with different linkage groups, including amine (yellow), thiomethyl (orange), and diphenylphosphino (purple), showed considerably higher rupture probabilities, which increase with an increasing applied voltage. This difference highlights the increased stability of a S–Au covalently linked junction under an applied electric field.

4.2 Special dative SH→Au contacts in self-assembled monolayers

Self-assembled monolayers (SAMs) are a powerful system for studying the interfacial properties of metals and semiconductors, and thiols and disulfides are the classic molecules for use in creating SAMs.[86–91] A study conducted by Inkpen *et al.* reached an intriguing postulation: when thiol-terminated compounds form SAMs on a gold surface, the interaction between the molecule and the gold substrate is predominantly through SH→Au dative bonds rather than S–Au covalent bonds.[79] As shown in the 1D histograms in Fig. 5g, single-molecule conductance measured for a solution of dodecane-1,12-dithiol is higher than that observed for SAMs of the same compound, suggesting different gold–sulfur binding mechanisms. As the conductance for covalently linked junctions is higher than that for junctions linked by dative bonds (Fig. 5e),[52] this observation suggests that in solution-based measurements, covalent S–Au bonds are formed as the hydrogen is displaced upon bond formation; conversely, in the SAM measurements, a dative

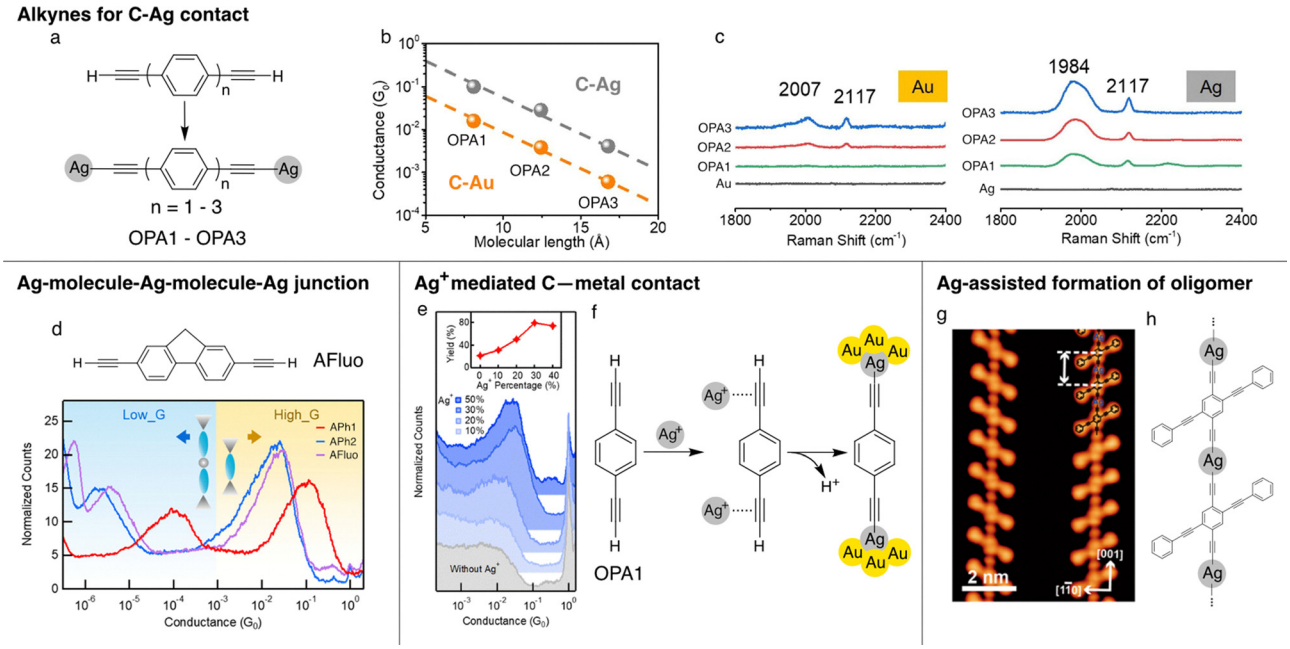

Fig. 6 (a) Chemical structures of **OPA1–OPA3** and the corresponding molecular junctions formed with Ag electrodes. (b) Conductance plotted against molecular length for **OPA1–OPA3** measured with Au (orange) and Ag (grey) electrodes. (c) Magnified SERS spectra of the relevant C≡C stretching regions (1800–2400 cm^{-1}) for **OPA1–OPA3** on Au (left) and Ag (right) in comparison to the results of metal surface only. (d) Chemical structure of **AFluo** and 1D logarithmically binned conductance histograms of **OPA1** (red), **OPA2** (blue), and **AFluo** (purple). (e) 1D conductance histograms of **OPA1** measured with 0–50% increasing amount of Ag^+ ions added in the solution. Inset: The yield of formed molecular junctions plotted as a function of Ag^+ ion percentage. (f) A schematic of Ag^+ ions-coupled *in situ* reaction. (g) High-resolution STM image of two organometallic chains on Ag (110) measured under 4.2 K and with a CO-modified tungsten tip. (h) The proposed chemical structure of the molecular chain. (b) and (c) are reprinted with permission from ref. 22, copyright (2020) American Chemical Society. (d) is reprinted with permission from ref. 71, copyright (2023) American Chemical Society. (e) is reprinted with permission from ref. 72, copyright (2023) The Royal Society of Chemistry. (g) is reprinted with permission from ref. 73, copyright (2015) American Chemical Society.

SH→Au bond is formed where hydrogen remains on the sulfur. The authors performed a series of experiments and showed substantial evidence that the SAMs formed on gold surfaces using thiols do not primarily consist of covalent S–Au bonds, but dative SH→Au contacts.

5. C–Ag covalent bonding by unprotected terminal acetylene

C–metal covalent linkage does not only occur with Au metal, but also with Ag. Having been applied as a metal contact for forming stable single-molecule junctions with various molecules,[19–21,23] silver has also been demonstrated to form C–Ag covalent linkages with organic structures. In 2020, Li *et al.*[22] reported that unprotected acetylene-terminated oligophenylenes spontaneously form robust and covalent –C≡C–Ag contacts with silver electrodes (Fig. 6a). By performing the STM-BJ experiments on **OPA1–OPA3**, the authors showed that the molecular conductance values for C–Ag linked junctions are nearly ten times those measured for C–Au linked junctions, as shown in Fig. 6b. The authors further extrapolated the data in Fig. 6b to zero molecular length and estimated the contact resistance of acetylene–Ag oligophenylene junctions to be 6 kΩ, which is significantly smaller than the one of acetylene–Au interfaces (36 kΩ). Surface-enhanced Raman spectroscopy (SERS) experiments provided direct evidence for the rapid formation of covalent C–Ag bonds.[22,61,92] As shown in Fig. 6c, for **OPA2** and **OPA3**, the bond signal $\nu(C\equiv C)_{bound}$ around 2000 cm^{-1} was observed on both Au and Ag substrates, which indicates the formation of covalent C–Au and C–Ag contacts (the peak at 2117 cm^{-1} is attributed to a C≡C stretching mode for unbound species).

In 2023, Song *et al.*[71] found that the molecular wires containing the –C≡C–Ag–C≡C– structure were likely formed when Ag was used as the STM electrode, a result of the strong organometallic C(sp)–Ag–C(sp) bonding between alkyne ligands and surface Ag atoms. In the 1D conductance histograms of **OPA1**, **OPA2**, and **AFluo** (Fig. 6d), two conductance peaks were observed for each molecule. The high_G state (yellow background) indicated that one molecule was connected between two Ag electrodes, and the low_G state (blue background) was explained as the formation of organometallic –C≡C–Ag–C≡C– wires driven by *in situ* coordination reactions. The authors performed DFT-based transport calculations and showed that the transmissions of the ligand junctions are ~3 orders of magnitude higher than those for the junctions composed of organometallic dimers, consistent with the STM-BJ experiment results.

Furthermore, the same research group developed a more flexible method to *in situ* construct similar organometallic nanostructures by supplying Ag^+ ions to the conductance measurements performed with Au electrodes.[72] In the absence of Ag^+ ions, the authors observed no well-defined molecular

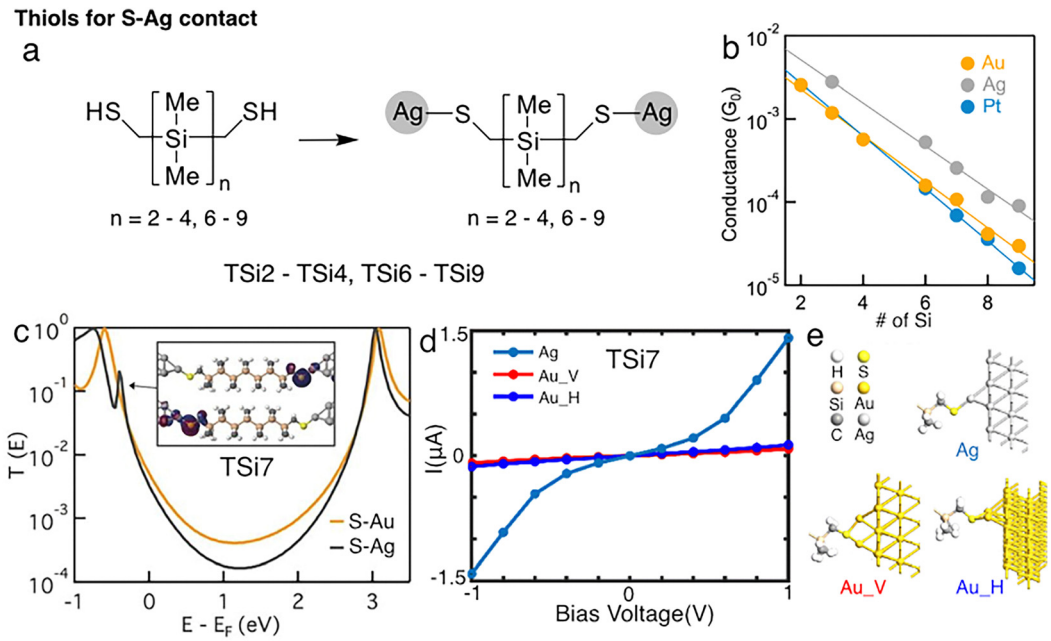

Fig. 7 (a) Chemical structures and formed molecular junctions of **TSi2–TSi4** and **TSi6–TSi9**. (b) Conductance plotted against the number of silicon atoms in the backbone for **TSi2–TSi4** and **TSi6–TSi9** measured with Au (orange), Ag (grey), and Pt (blue) electrodes, and lines showing linear fits to the data following the $G = G_C e^{-\beta n}$ equation. (c) Calculated transmission curves for Au–**TSi7**–Au (orange) and Ag–**TSi7**–Ag (grey) junctions. Inset: Gateway state orbitals. (d) Calculated current–voltage curves of Au–**TSi7**–Au and Ag–**TSi7**–Ag junctions. Two binding configurations V and H for Au–**TSi7**–Au junctions are included in the calculation. (e) Optimized geometric structures of molecular junctions for the Ag(111) electrode with one protruding Ag atom surface, and Au(111) electrode with the vertical/horizontal configuration of a double atomic surface (Au_V/Au_H). (b) and (c) are adapted with permission from ref. 21, copyright (2017) Wiley-VCH. (d) and (e) are adapted with permission from ref. 96, copyright (2023) The Royal Society of Chemistry.

conductance peak for **OPA1** measured with Au electrodes, as shown in Fig. 6e, grey line. However, after a dilute solution of silver salt $AgPF_6$ was added to the molecular solution, clear molecular conductance plateaus appeared at $\sim 10^{-2}G_0$, suggesting that the introduction of Ag^+ ions facilitated the formation of single **OPA1** molecular junctions. The authors proposed that the Ag^+ ion-coupled *in situ* reaction with **OPA1** results in –C≡C–Ag bond formation, and the robust C–Ag contact is anchored on the surface of the Au electrodes by metallic bonding, and thus an Au/Ag–molecule–Ag/Au junction is formed, as illustrated in Fig. 6f.

Years before the establishment of C–Ag contact in STM-BJ experiments, one-dimensional organometallic chains formed with covalent C–Ag bonds on Ag(110) surfaces were observed under 4.2 K by STM in 2015.[73] A high-resolution STM image of the 1D chains (Fig. 6g) showed that a round dot was located between two adjacent molecules and was connected to the nearby molecules by alkynyl groups, indicating the involvement of Ag atoms in the chain formation (chemical structure of the 1D chain in Fig. 6h). The perfect match between the periodicity of the organometallic chain and the Ag(110) substrate lattice constant, as well as the robust C–Ag contact, taken together, result in the formation of the stable organometallic products.

In summary, C–Ag contacts form spontaneously under ambient conditions. The use of Ag metal (or Au metal with Ag^+ ions) provides strategies to create unconventional molecule–metal interfaces and opens new avenues for building molecular wires with low contact resistance.

6. S–Ag covalent bonding from thiol-terminated silanes

Besides the C–Ag covalent contact, another S–Ag covalent bond has also been established for linking molecules with Ag electrodes. In 2017, Li *et al.*[21] measured a series of thiol-terminated silanes (structures in Fig. 7a) using the STM-BJ technique and first demonstrated that the S–Ag linked silane junctions display a higher conductance than those of S–Au linked ones. Single molecule junction conductance as a function of the number of silicon atoms in the backbone for silanes connected with Au, Ag, and Pt electrodes through thiol linker groups, are shown in Fig. 7b. We see that junctions with S–Ag covalent contacts show a conductance ~3 times those for S–Au or S–Pt linked ones. In the calculated transmission curves of junctions of **TSi7** bound to Au (orange line) and Ag (grey line), as shown in Fig. 7c, an extra resonance appeared at 400 meV below the Fermi energy in Ag-based junctions, but this feature was not visible as a separate resonance in the transmission for Au-linked junctions. This resonance peak is attributed to a S–Ag orbital gateway state (inset

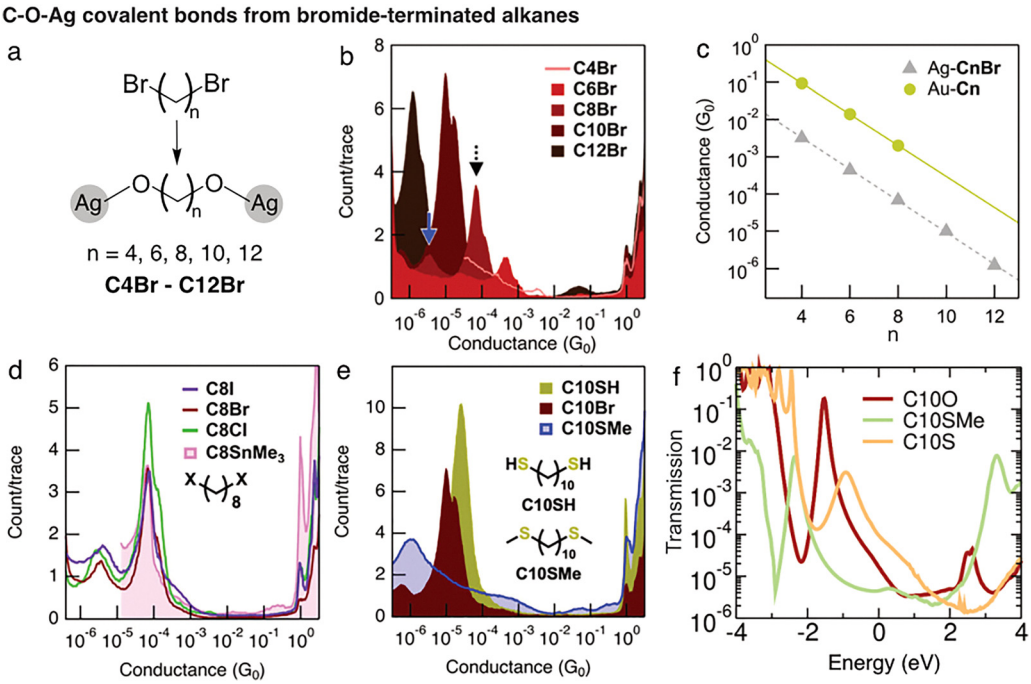

Fig. 8 (a) Chemical structures of **C4Br–C12Br** and their corresponding molecular junctions formed with Ag electrodes. (b) Overlaid 1D histograms obtained of 0.1 mM **C*n*Br** solutions in tetradecane at 750 mV bias (*n* = 4–12) with Ag electrodes. The arrows indicate assigned high (black dotted) and low (blue solid) conductance peaks for **C8Br**. (c) A plot of conductance *versus* number of repeat units (*n*) for alkane junctions comprising covalent C–Au linkages (Au–**C*n***) (gold circles, solid line) and proposed C–O–Ag linkages (silver triangles, dashed line). The conductance for the proposed C–O–Ag linked junctions was determined from the main conductance features observed for Ag–**C*n*Br** junctions shown in Fig. 9(b). (d) 1D histograms for iodide- (**C8I**, purple), bromide- (**C8Br**, red), chloride- (**C8Cl**, green), and trimethylstannyl-terminated (**C8SnMe3**, pink) 1,8-octane wires measured with Ag electrodes. (e) Overlaid 1D histograms for **C10SH**, **C10Br**, and **C10SMe** measured with Ag electrodes. (f) Calculated transmission spectra of **C10** junctions with two oxygen (**C10O**), thiomethyl (**C10SMe**), and thiol (**C10S**) terminations attached to Ag electrodes. (b)–(f) are reprinted with permission from ref. 56, copyright (2024) American Chemical Society.

in Fig. 7c), which has been observed in calculations of other covalent metal–organic contacts such as C–Au and S–Au bonds,[93–95] though sometimes the gateway state is not as prominent due to broadening of the nearby frontier orbitals.

Recently, Wang *et al.*[96] further investigated these junctions through first-principles calculations and found that the interfacial configuration difference is possibly the main reason for the observed higher conductance for S–Ag linked silane junctions than that of S–Au linked ones. As an example shown in Fig. 7d, in the applied voltage range of −1 V to 1 V, the current of the Ag–**TSi7**–Ag molecular junction (blue) increased approximately exponentially when the applied bias voltage was increased, while that of the Au–**TSi7**–Au junction (red and purple for two binding geometries) only slightly increased, almost linearly. In particular, the authors identified quite different atomic configurations for the Ag and Au electrodes. Ag forms a monoatomic point contact whereas Au preferentially forms a double-atomic contact with two binding geometries vertical or horizontal to the silane backbone (illustrated in Fig. 7e). Although it is difficult to test the metal atomic configuration experimentally, different properties such as snap backs and molecular junction elongation lengths have been observed between Au- and Ag-linked junctions.[19,21] The authors further showed that in comparison to S–Au, the S–Ag interface state is closer to the Fermi level, and thus more likely to enter the bias window to contribute a higher junction current.

In these examples of a silicon chain as the backbone, covalent S–Ag contacts are more conductive than S–Au contacts when metal–molecule–metal junctions are formed under ambient conditions. The calculations of the S–Ag linked systems provide further insight into the different configurations of the S–Au and S–Ag contacts and how these conformational differences affect the transport properties of molecular junctions.

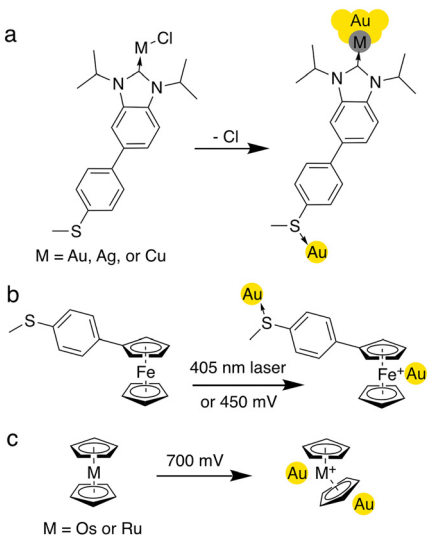

Fig. 9 (a) Schematic illustration of *in situ* electrochemical reduction of NHC–M–Cl complexes in forming C–M–Au bonds. (b) Formation of an Fe–Au bond in single-molecule junctions upon oxidation of ferrocene by a 405 nm laser or 450 mV applied voltage in an ionic solution. (c) Formation of oxidized ruthenocene and osmocene junctions in a polar solvent environment through Au–metal bonds on one end and an Au–π interaction on the other.

7. C–O–Ag bonding from α,ω-alkanedibromides under an inert atmosphere

Recently, Czyszczon-Burton T. M. *et al.*[56] reported a new C–O–Ag covalent contact formed from the reaction of chemisorbed alkyls with co-adsorbed oxygens on the silver surface. The authors performed conductance measurements of a series of α,ω-alkanedibromides (chemical structures are shown in Fig. 8a) with silver electrodes using an STM-BJ setup housed inside an inert atmosphere glovebox. Comparing the main conductance state for Ag–C*n*Br junctions (black dotted arrow, Fig. 8b) with the alkane junctions comprising covalent C–Au linkages, these two families of junctions differ in conductance by a factor of ∼30 (Fig. 8c).

Octanes with iodide, bromide, chloride, and trimethylstannyl terminal groups (**C8I**, **C8Br**, **C8Cl**, and **C8SnMe3**) were studied, and the major conductance states for these four molecules were found to be nearly identical, as shown in Fig. 8d. The authors concluded that the junctions in each case result from the *in situ* cleavage of the terminal groups to form junctions of similar composition and geometry, particularly given that the trimethylstannyl group had been demonstrated to cleave in forming a covalent C–Au contact with Au electrodes.[47] In addition, the conductance of **C10Br** junctions is intermediate between junctions comprising physisorbed (**C10SMe**) and chemisorbed (**C10SH**) sulfur linkers, as shown in Fig. 8e. Taken together, given the low junction conductance observed experimentally, the authors proposed that in measurements of α,ω-alkanedibromides, **C8I**, **C8Cl**, and **C8SnMe3**, alkoxides (**C*n*O**) on the silver surface were trapped and measured, comprising an interfacial C(sp^3)–O–Ag contact, which is expected to be less conducting than the C(sp^3)–Ag contact. As it was a great challenge to provide direct experimental evidence to confirm this hypothesis, the authors performed density functional theory (DFT) calculations to evaluate the conductance of C–O–Ag linked junctions. Notably, for junctions formed with silver electrodes, the calculated conductance for the **C10O** (Fig. 8f) junction lies between the computed values for **C10SMe** and **C10S** junctions, which agrees with the experimental results seen for **C10Br**, **C10SMe**, and **C10SH**, supporting the C–O–Ag contact proposition.

8. Emerging novel bonding strategies

In addition to covalent metal–molecule interactions, alternative robust interfacial bonding strategies have emerged. N-Heterocyclic carbenes (NHCs), neutral divalent carbon ligands with a six-electron configuration, have been shown to form stable bonds with metal surfaces.[97–99] NHC–M–Au (M = Au, Ag, and Cu) interfacial moieties were generated by electrochemical reduction of NHC–M–Cl complexes under ambient conditions,

achieving enhanced binding strength compared to traditional dative linkages (Fig. 9a).[44] This study enables investigation into the electronic properties of a broad range of carbene–electrode interfaces, including those involving heterometallic contacts.

Another type of robust binding scheme is metal–metal bond, which has been realized by the use of metallocenes with gold electrodes.[41–43] Specifically, ferrocene derivatives, either through photooxidation by 405 nm light irradiation or through electrochemical oxidation under a high applied bias voltage, have been shown to bind to Au electrodes by metal–metal bonds between the formal Fe^{3+} centers (oxidized ferrocene contains a formal Fe^{3+} center and neutral ferrocene contains a formal Fe^{2+} center) and Au electrodes (Fig. 9b).[42] A similar approach has been applied for creating metal–metal contacts between other metallocenes, such as ruthenocenes and osmocenes, and Au electrodes.[43] Ruthenocenes and osmocenes have been demonstrated to form single-molecule junctions through a direct Au–π interaction on one side and an Au–metal bond on the other when the metal center is oxidized by a high applied bias voltage (Fig. 9c). The authors suggested that upon oxidation of the metallocene, one cyclopentadienyl ring undergoes slippage isomerization, which is a critical step for enabling the metal–metal contact on one side and Au–π coupling on the other.

9. Conclusion and outlook

Covalent bonding between molecules and metal electrodes offers exciting possibilities for the development of stable and robust nanoscale devices. We provide a comprehensive overview of chemical reactions that enable the formation of covalent bonds between molecules and metal surfaces. Chemical reactions have facilitated the formation of molecule–gold linkages of C–Au, N–Au, and S–Au bonds, as well as molecule–silver linkages of C–Ag, S–Ag, and C–O–Ag bonds. These discoveries not only expand the types of linkers that we can use in creating molecular electronic devices, but also provide appealing examples of chemical reactions that occur when organic compounds bridge nanogaps between metal contacts under an applied electric field.

In some of the systems where reactions occur at the molecule/metal interface for forming novel linkages, additional reactions can further be induced in generating new organic species[47,52,53,57] and organometallic chains.[71] Such developments, on the other hand, also motivated studies on forming molecule–metal contacts under an inert atmosphere to eliminate reactions or promote alternative reactions.[25,56,100] Cryogenic temperature, which is considered to hinder chemical reactions, has also been applied in studies of metal–molecule–metal junctions.[24,101,102]

Looking ahead, new covalent molecule–metal linkages will continue to be discovered. Given the fact that covalent anchoring moieties enable highly conductive junctions in some structures[47,48,52,93] while yielding conductance similar to the dative-bonded analogs in others,[53,57] it is critical for researchers to investigate various backbones for identifying the chemical principles that guide these conductance properties. For example, for the C–Au bond, carbon could be either sp^3, sp^2, or sp hybridized, and this carbon could also be part of a π-conjugated structure such as a benzene; all of these could influence the overall charge transport properties, and thus there might not be the same C–Au contact resistance for all junctions.

Moreover, *in situ* characterization techniques combined with the break-junction technique can enable *in situ* identification of the formation of a covalent bond and new chemical species in confined nanoscale environments, potentially providing further information about the reaction mechanism. To exemplify, single-molecule surface-enhanced Raman spectroscopy (SERS) and tip-enhanced Raman spectroscopy (TERS) have been demonstrated to show capabilities in resolving molecular-scale reactions and real-time tracking of bond evolution at nanoscale interfaces,[103,104] and *in situ* Raman spectroscopy has been successfully implemented in break-junction experiments.[105–107] Additionally, covalent linkages have been utilized for constructing molecular rectifiers[94,108] and high power factor (GS^2, G is the conductance and S is the Seebeck coefficient) electronic components.[93] The robust binding by the covalent bond between the molecule and Au electrodes also enables molecular switches under mechanical modulation, as shown in the demonstration of switching events between closed and open ring forms of spiropyran and merocyanine attached to Au electrodes.[109] With increasing integration of covalent molecule–metal interactions into molecular device architectures, these findings will guide the future design of molecular electronic components.

Conflicts of interest

There are no conflicts to declare.

Data availability

No primary research results, software, or code have been included and no new data were generated or analysed as part of this review article.

Acknowledgements

H. L. acknowledges the support of the Research Grants Council of the Hong Kong SAR, China (project no. 21310722 and 11304723) and the City University of Hong Kong through a start-up fund (9610521) and a Strategic Interdisciplinary Research Grant (7020095).

References

1 S. V. Aradhya and L. Venkataraman, *Nat. Nanotechnol.*, 2013, **8**, 399–410.
2 F. Chen, J. Hihath, Z. Huang, X. Li and N. Tao, *Annu. Rev. Phys. Chem.*, 2007, **58**, 535–564.

3 M. Ratner, *Nat. Nanotechnol.*, 2013, **8**, 378–381.
4 N. Xin, J. Guan, C. Zhou, X. Chen, C. Gu, Y. Li, M. A. Ratner, A. Nitzan, J. F. Stoddart and X. Guo, *Nat. Rev. Phys.*, 2019, **1**, 211–230.
5 C. Yan, C. Fang, J. Gan, J. Wang, X. Zhao, X. Wang, J. Li, Y. Zhang, H. Liu, X. Li, J. Bai, J. Liu and W. Hong, *ACS Nano*, 2024, **18**, 28531–28556.
6 B. Xu and N. J. Tao, *Science*, 2003, **301**, 1221–1223.
7 L. Venkataraman, J. E. Klare, I. W. Tam, C. Nuckolls, M. S. Hybertsen and M. L. Steigerwald, *Nano Lett.*, 2006, **6**, 458–462.
8 J. Van Ruitenbeek, A. Alvarez, I. Piñeyro, C. Grahmann, P. Joyez, M. Devoret, D. Esteve and C. Urbina, *Rev. Sci. Instrum.*, 1996, **67**, 108–111.
9 J. Reichert, R. Ochs, D. Beckmann, H. Weber, M. Mayor and H. von Löhneysen, *Phys. Rev. Lett.*, 2002, **88**, 1–4.
10 G. Gryn'ova and C. Corminboeuf, *Chimia*, 2019, **73**, 245.
11 D. C. Milan, A. Vezzoli, I. J. Planje and P. J. Low, *Dalton Trans.*, 2018, **47**, 14125–14138.
12 S. J. Higgins and R. J. Nichols, *Polyhedron*, 2018, **140**, 25–34.
13 T. C. Siu, J. Y. Wong, M. O. Hight and T. A. Su, *Phys. Chem. Chem. Phys.*, 2021, **23**, 9643–9659.
14 X. Xiao, B. Xu and N. Tao, *J. Am. Chem. Soc.*, 2004, **126**, 5370–5371.
15 J. Juhaniewicz and S. Sek, *Bioelectrochemistry*, 2012, **87**, 21–27.
16 J. M. Brisendine, S. Refaely-Abramson, Z.-F. Liu, J. Cui, F. Ng, J. B. Neaton, R. L. Koder and L. Venkataraman, *J. Phys. Chem. Lett.*, 2018, **9**, 763–767.
17 J. M. Artés, Y. Li, J. Qi, M. Anantram and J. Hihath, *Nat. Commun.*, 2015, **6**, 8870.
18 C. Guo, K. Wang, E. Zerah-Harush, J. Hamill, B. Wang, Y. Dubi and B. Xu, *Nat. Chem.*, 2016, **8**, 484–490.
19 T. Kim, H. Vázquez, M. S. Hybertsen and L. Venkataraman, *Nano Lett.*, 2013, **13**, 3358–3364.
20 S. Kaneko, T. Nakazumi and M. Kiguchi, *J. Phys. Chem. Lett.*, 2010, **1**, 3520–3523.
21 H. Li, T. A. Su, M. Camarasa-Gómez, D. Hernangómez-Pérez, S. E. Henn, V. Pokorný, C. D. Caniglia, M. S. Inkpen, R. Korytár, M. L. Steigerwald, C. Nuckolls, F. Evers and L. Venkataraman, *Angew. Chem., Int. Ed.*, 2017, **56**, 14145–14148.
22 S. Li, H. Yu, X. Chen, A. A. Gewirth, J. S. Moore and C. M. Schroeder, *Nano Lett.*, 2020, **20**, 5490–5495.
23 X.-Y. Zhou, Y.-H. Wang, H.-M. Qi, J.-F. Zheng, Z.-J. Niu and X.-S. Zhou, *Nanoscale Res. Lett.*, 2014, **9**, 1–6.
24 T. Yelin, R. Korytár, N. Sukenik, R. Vardimon, B. Kumar, C. Nuckolls, F. Evers and O. Tal, *Nat. Mater.*, 2016, **15**, 444–449.
25 T. M. Czyszczonr.es. L, S. Lazar, Z. Miao and M. S. Inkpen, *Small*, 2025, 2502972.
26 T. M. Czyszczon-Burton, E. Montes, J. Prana, S. F. Chen, C. P. Pakhanyan, H. Vázquez and M. S. Inkpen, *Nano Lett.*, 2025, **25**, 9125–9131.
27 R. Smit, Y. Noat, C. Untiedt, N. Lang, M. V. van Hemert and J. Van Ruitenbeek, *Nature*, 2002, **419**, 906–909.
28 C.-H. Ko, M.-J. Huang, M.-D. Fu and C.-H. Chen, *J. Am. Chem. Soc.*, 2010, **132**, 756–764.
29 D.-F. Li, J.-C. Mao, D.-L. Chen, F. Chen, H. Ze-Wen, X.-Y. Zhou, Y.-H. Wang, X.-S. Zhou, Z.-J. Niu and E. Maisonhaute, *Electrochim. Acta*, 2015, **174**, 340–344.
30 X.-S. Zhou, J.-H. Liang, Z.-B. Chen and B.-W. Mao, *Electrochem. Commun.*, 2011, **13**, 407–410.
31 R. J. Nichols and S. J. Higgins, *Acc. Chem. Res.*, 2016, **49**, 2640–2648.
32 R. J. Brooke, C. Jin, D. S. Szumski, R. J. Nichols, B.-W. Mao, K. S. Thygesen and W. Schwarzacher, *Nano Lett.*, 2015, **15**, 275–280.
33 Y.-H. Wang, X.-Y. Zhou, Y.-Y. Sun, D. Han, J.-F. Zheng, Z.-J. Niu and X.-S. Zhou, *Electrochim. Acta*, 2014, **123**, 205–210.
34 H. Haick and D. Cahen, *Prog. Surf. Sci.*, 2008, **83**, 217–261.
35 V. Kaliginedi, A. V. Rudnev, P. Moreno-García, M. Baghernejad, C. Huang, W. Hong and T. Wandlowski, *Phys. Chem. Chem. Phys.*, 2014, **16**, 23529–23539.
36 H. Liu, H. Zhang, Y. Zhao, J. Liu and W. Hong, *Trends Chem.*, 2023, **5**, 367–379.
37 S. V. Aradhya, M. Frei, M. S. Hybertsen and L. Venkataraman, *Nat. Mater.*, 2012, **11**, 872–876.
38 Y. Wei, L. Li, J. E. Greenwald and L. Venkataraman, *Nano Lett.*, 2023, **23**, 567–572.
39 M. Huang, M. Sun, X. Yu, S. He, S. Liu, W. M. Nau, Y. Li, T. Wu, Y. Wang, S. Chang and J. He, *J. Phys. Chem. C*, 2020, **124**, 16143–16148.
40 K. Kanthasamy, M. Ring, D. Nettelroth, C. Tegenkamp, H. Butenschön, F. Pauly and H. Pfnür, *Small*, 2016, **12**, 4849–4856.
41 B. Pabi, Š. Marek, A. Pal, P. Kumari, S. J. Ray, A. Thakur, R. Korytár and A. N. Pal, *Nanoscale*, 2023, **15**, 12995–13008.
42 W. Lee, L. Li, M. Camarasa-Gómez, D. Hernangómez-Pérez, X. Roy, F. Evers, M. S. Inkpen and L. Venkataraman, *Nat. Commun.*, 2024, **15**, 1439.
43 W. Lee, C. R. Prindle, W. Shi, S. Louie, M. L. Steigerwald and L. Venkataraman, *Nano Lett.*, 2025, **25**, 3316–3322.
44 E. A. Doud, M. S. Inkpen, G. Lovat, E. Montes, D. W. Paley, M. L. Steigerwald, H. Vázquez, L. Venkataraman and X. Roy, *J. Am. Chem. Soc.*, 2018, **140**, 8944–8949.
45 A. Inayeh, R. R. Groome, I. Singh, A. J. Veinot, F. C. de Lima, R. H. Miwa, C. M. Crudden and A. B. McLean, *Nat. Commun.*, 2021, **12**, 4034.
46 E. Amit, L. Dery, S. Dery, S. Kim, A. Roy, Q. Hu, V. Gutkin, H. Eisenberg, T. Stein, D. Mandler, F. Dean Toste and E. Gross, *Nat. Commun.*, 2020, **11**, 5714.
47 Z.-L. Cheng, R. Skouta, H. Vazquez, J. R. Widawsky, S. Schneebeli, W. Chen, M. S. Hybertsen, R. Breslow and L. Venkataraman, *Nat. Nanotechnol.*, 2011, **6**, 353–357.
48 W. Chen, J. R. Widawsky, H. Vázquez, S. T. Schneebeli, M. S. Hybertsen, R. Breslow and L. Venkataraman, *J. Am. Chem. Soc.*, 2011, **133**, 17160–17163.
49 S. Ghasemi and K. Moth-Poulsen, *Nanoscale*, 2021, **13**, 659–671.

50 X. Guo, J. P. Small, J. E. Klare, Y. Wang, M. S. Purewal, I. W. Tam, B. H. Hong, R. Caldwell, L. Huang, S. O'Brien, J. Yan, R. Breslow, S. J. Wind, J. Hone, P. Kim and C. Nuckolls, *Science*, 2006, **311**, 356–359.
51 C. Jia, A. Migliore, N. Xin, S. Huang, J. Wang, Q. Yang, S. Wang, H. Chen, D. Wang, B. Feng, Z. Liu, G. Zhang, D.-H. Qu, H. Tian, M. A. Ratner, H. Q. Xu, A. Nitzan and X. Guo, *Science*, 2016, **352**, 1443–1445.
52 R. L. Starr, T. Fu, E. A. Doud, I. Stone, X. Roy and L. Venkataraman, *J. Am. Chem. Soc.*, 2020, **142**, 7128–7133.
53 Y. Li, C. Zhao, R. Wang, A. Tang, W. Hong, D. Qu, H. Tian and H. Li, *CCS Chem.*, 2023, **5**, 191–199.
54 L. Kim, T. M. Czyszczon-Burton, K. M. Nguyen, S. Stukey, S. Lazar, J. Prana, Z. Miao, S. Park, S. F. Chen and M. S. Inkpen, *Nano Lett.*, 2024, **24**, 9998–10005.
55 M. Zhang, J. Lin, K. Song, K. Chang, X. Dai, Y. Zang and D. Zhu, *J. Am. Chem. Soc.*, 2023, **145**, 6480–6485.
56 T. M. Czyszczon-Burton, E. Montes, J. Prana, S. Lazar, N. Rotthowe, S. F. Chen, H. Vázquez and M. S. Inkpen, *J. Am. Chem. Soc.*, 2024, **146**, 28516–28526.
57 W. Guo, Y. Wu, C. Xie, X. Tan, Z. Lu and H. Li, *J. Am. Chem. Soc.*, 2024, **146**, 26687–26693.
58 X. Yao, M. Vonesch, M. Combes, J. Weiss, X. Sun and J.-C. Lacroix, *Nano Lett.*, 2021, **21**, 6540–6548.
59 T. Hines, I. Díez-Pérez, H. Nakamura, T. Shimazaki, Y. Asai and N. Tao, *J. Am. Chem. Soc.*, 2013, **135**, 3319–3322.
60 C. R. Peiris, Y. B. Vogel, A. P. Le Brun, A. C. Aragonès, M. L. Coote, I. Díez-Pérez, S. Ciampi and N. Darwish, *J. Am. Chem. Soc.*, 2019, **141**, 14788–14797.
61 W. Hong, H. Li, S.-X. Liu, Y. Fu, J. Li, V. Kaliginedi, S. Decurtins and T. Wandlowski, *J. Am. Chem. Soc.*, 2012, **134**, 19425–19431.
62 C. Huang, S. Chen, K. Baruël Ørnsø, D. Reber, M. Baghernejad, Y. Fu, T. Wandlowski, S. Decurtins, W. Hong, K. S. Thygesen and S.-X. Liu, *Angew. Chem., Int. Ed.*, 2015, **54**, 14304–14307.
63 I. J. Olavarria-Contreras, M. L. Perrin, Z. Chen, S. Klyatskaya, M. Ruben and H. S. J. van der Zant, *J. Am. Chem. Soc.*, 2016, **138**, 8465–8469.
64 F. Bejarano, I. J. Olavarria-Contreras, A. Droghetti, I. Rungger, A. Rudnev, D. Gutiérrez, M. Mas-Torrent, J. Veciana, H. S. J. van der Zant, C. Rovira, E. Burzuri and N. Crivillers, *J. Am. Chem. Soc.*, 2018, **140**, 1691–1696.
65 P. Pla-Vilanova, A. C. Aragonès, S. Ciampi, F. Sanz, N. Darwish and I. Diez-Perez, *Nanotechnology*, 2015, **26**, 381001.
66 J. Lin, Y. Lv, K. Song, X. Song, H. Zang, P. Du, Y. Zang and D. Zhu, *Nat. Commun.*, 2023, **14**, 293.
67 Y. Zang, A. Pinkard, Z.-F. Liu, J. B. Neaton, M. L. Steigerwald, X. Roy and L. Venkataraman, *J. Am. Chem. Soc.*, 2017, **139**, 14845–14848.
68 J. Prana, L. Kim, T. M. Czyszczon-Burton, G. Homann, S. F. Chen, Z. Miao, M. Camarasa-Gómez and M. S. Inkpen, *J. Am. Chem. Soc.*, 2024, **146**, 33265–33275.
69 J. Prana, L. Zagami, K. Yan, D. Hernangómez-Pérez, M. Camarasa-Gómez and M. S. Inkpen, *Nano Lett.*, 2025, **25**, 10427–10434.
70 U. Rashid, M. Bro-Jørgensen, K. B. Harilal, P. A. Sreelakshmi, R. R. Mondal, V. Chittari Pisharam, K. N. Parida, K. Geetharani, J. M. Hamill and V. Kaliginedi, *J. Am. Chem. Soc.*, 2024, **146**, 9063–9073.
71 K. Song, J. Lin, X. Song, M. Zhang, Q. Gu, Y. Zang and D. Zhu, *J. Phys. Chem. C*, 2023, **127**, 8850–8855.
72 K. Song, J. Lin, X. Song, B. Yang, J. Zhu, Y. Zang and D. Zhu, *Chem. Commun.*, 2023, **59**, 6207–6210.
73 J. Liu, Q. Chen, L. Xiao, J. Shang, X. Zhou, Y. Zhang, Y. Wang, X. Shao, J. Li, W. Chen, G. Q. Xu, H. Tang, D. Zhao and K. Wu, *ACS Nano*, 2015, **9**, 6305–6314.
74 R. Ahmad, L. Boubekeur-Lecaque, M. Nguyen, S. Lau-Truong, A. Lamouri, P. Decorse, A. Galtayries, J. Pinson, N. Felidj and C. Mangeney, *J. Phys. Chem. C*, 2014, **118**, 19098–19105.
75 L. Venkataraman, J. E. Klare, C. Nuckolls, M. S. Hybertsen and M. L. Steigerwald, *Nature*, 2006, **442**, 904–907.
76 M. S. Hybertsen, L. Venkataraman, J. E. Klare, A. C. Whalley, M. L. Steigerwald and C. Nuckolls, *J. Phys.: Condens. Matter*, 2008, **20**, 374115.
77 M. S. Hybertsen and L. Venkataraman, *Acc. Chem. Res.*, 2016, **49**, 452–460.
78 H. Li, T. A. Su, V. Zhang, M. L. Steigerwald, C. Nuckolls and L. Venkataraman, *J. Am. Chem. Soc.*, 2015, **137**, 5028–5033.
79 M. S. Inkpen, Z. F. Liu, H. Li, L. M. Campos, J. B. Neaton and L. Venkataraman, *Nat. Chem.*, 2019, **11**, 351–358.
80 M. A. Reed, C. Zhou, C. J. Muller, T. P. Burgin and J. M. Tour, *Science*, 1997, **278**, 252–254.
81 T. A. Su, M. Neupane, M. L. Steigerwald, L. Venkataraman and C. Nuckolls, *Nat. Rev. Mater.*, 2016, **1**, 16002.
82 J. Ponce, C. R. Arroyo, S. Tatay, R. Frisenda, P. Gaviña, D. Aravena, E. Ruiz, H. S. J. van der Zant and E. Coronado, *J. Am. Chem. Soc.*, 2014, **136**, 8314–8322.
83 F. Schwarz, M. Koch, G. Kastlunger, H. Berke, R. Stadler, K. Venkatesan and E. Lörtscher, *Angew. Chem., Int. Ed.*, 2016, **55**, 11781–11786.
84 V. Kolivoska, P. Moreno-García, V. Kaliginedi, W. Hong, M. Mayor, N. Weibel and T. Wandlowski, *Electrochim. Acta*, 2013, **110**, 709–717.
85 R. Frisenda, S. Tarkuç, E. Galán, M. L. Perrin, R. Eelkema, F. C. Grozema and H. S. van der Zant, *Beilstein J. Nanotechnol.*, 2015, **6**, 1558–1567.
86 E. M. Dief and N. Darwish, *ACS Sens.*, 2021, **6**, 573–580.
87 E. M. Dief and N. Darwish, *Chem. Sci.*, 2023, **14**, 3428–3440.
88 C. R. Peiris, S. Ciampi, E. M. Dief, J. Zhang, P. J. Canfield, A. P. Le Brun, D. S. Kosov, J. R. Reimers and N. Darwish, *Chem. Sci.*, 2020, **11**, 5246–5256.
89 J. C. Love, L. A. Estroff, J. K. Kriebel, R. G. Nuzzo and G. M. Whitesides, *Chem. Rev.*, 2005, **105**, 1103–1170.
90 C. Jung, O. Dannenberger, Y. Xu, M. Buck and M. Grunze, *Langmuir*, 1998, **14**, 1103–1107.
91 C. D. Bain, H. A. Biebuyck and G. M. Whitesides, *Langmuir*, 1989, **5**, 723–727.
92 S. W. Joo and K. Kim, *J. Raman Spectrosc.*, 2004, **35**, 549–554.

93 J. R. Widawsky, W. Chen, H. Vázquez, T. Kim, R. Breslow, M. S. Hybertsen and L. Venkataraman, *Nano Lett.*, 2013, **13**, 2889–2894.
94 A. Batra, P. Darancet, Q. Chen, J. S. Meisner, J. R. Widawsky, J. B. Neaton, C. Nuckolls and L. Venkataraman, *Nano Lett.*, 2013, **13**, 6233–6237.
95 S. Sangtarash, A. Vezzoli, H. Sadeghi, N. Ferri, H. M. O'Brien, I. Grace, L. Bouffier, S. J. Higgins, R. J. Nichols and C. J. Lambert, *Nanoscale*, 2018, **10**, 3060–3067.
96 M. Wang, X. Chen, W. Lu, X. Tian and G.-P. Zhang, *Phys. Chem. Chem. Phys.*, 2023, **25**, 13673–13682.
97 A. V. Zhukhovitskiy, M. G. Mavros, T. Van Voorhis and J. A. Johnson, *J. Am. Chem. Soc.*, 2013, **135**, 7418–7421.
98 C. M. Crudden, J. H. Horton, I. I. Ebralidze, O. V. Zenkina, A. B. McLean, B. Drevniok, Z. She, H.-B. Kraatz, N. J. Mosey, T. Seki, E. C. Keske, J. D. Leake, A. Rousina-Webb and G. Wu, *Nat. Chem.*, 2014, **6**, 409–414.
99 C. M. Crudden, J. H. Horton, M. R. Narouz, Z. Li, C. A. Smith, K. Munro, C. J. Baddeley, C. R. Larrea, B. Drevniok, B. Thanabalasingam, A. B. McLean, O. V. Zenkina, I. I. Ebralidze, Z. She, H.-B. Kraatz, N. J. Mosey, L. N. Saunders and A. Yagi, *Nat. Commun.*, 2016, **7**, 12654.
100 Y. Li, M. Buerkle, G. Li, A. Rostamian, H. Wang, Z. Wang, D. R. Bowler, T. Miyazaki, L. Xiang, Y. Asai, G. Zhou and N. Tao, *Nat. Mater.*, 2019, **18**, 357–363.
101 B. Lawson, P. Zahl, M. S. Hybertsen and M. Kamenetska, *J. Am. Chem. Soc.*, 2022, **144**, 6504–6515.
102 M. Kamenetska, J. R. Widawsky, M. Dell'Angela, M. Frei and L. Venkataraman, *J. Chem. Phys.*, 2017, **146**, 092311.
103 A. B. Zrimsek, N. Chiang, M. Mattei, S. Zaleski, M. O. McAnally, C. T. Chapman, A.-I. Henry, G. C. Schatz and R. P. Van Duyne, *Chem. Rev.*, 2017, **117**, 7583–7613.
104 H.-K. Choi, K. S. Lee, H.-H. Shin, J.-J. Koo, G. J. Yeon and Z. H. Kim, *Acc. Chem. Res.*, 2019, **52**, 3008–3017.
105 J.-H. Tian, B. Liu, X. Li, Z.-L. Yang, B. Ren, S.-T. Wu, N. Tao and Z.-Q. Tian, *J. Am. Chem. Soc.*, 2006, **128**, 14748–14749.
106 D. R. Ward, N. J. Halas, J. W. Ciszek, J. M. Tour, Y. Wu, P. Nordlander and D. Natelson, *Nano Lett.*, 2008, **8**, 919–924.
107 C. Tang, M. Su, T. Lu, J. Zheng, J. Wang, Y. Zhou, Y.-L. Zou, W. Liu, R. Huang, W. Xu, L. Chen, Y. Zhang, J. Bai, Y. Yang, J. Shi, J. Liu and W. Hong, *Chem. Sci.*, 2024, **15**, 13486–13494.
108 M. Koepf, C. Koenigsmann, W. Ding, A. Batra, C. F. A. Negre, L. Venkataraman, G. W. Brudvig, V. S. Batista, C. A. Schmuttenmaer and R. H. Crabtree, *Nanoscale*, 2016, **8**, 16357–16362.
109 M. C. Walkey, C. R. Peiris, S. Ciampi, A. C. Aragonès, R. B. Domínguez-Espíndola, D. Jago, T. Pulbrook, B. W. Skelton, A. N. Sobolev, I. Díez Pérez, M. J. Piggott, G. A. Koutsantonis and N. Darwish, *ACS Appl. Mater. Interfaces*, 2019, **11**, 36886–36894.

